JOURNAL OF GEOPHYSICAL RESEARCH, VOL. 100, NO. D2, PAGES 2817–2831, FEBRUARY 20, 1995

Land-atmosphere CO_2 exchange simulated by a land surface process model coupled to an atmospheric general circulation model

Gordon B. Bonan
National Center for Atmospheric Research, Boulder, Colorado

Abstract. CO_2 uptake during plant photosynthesis and CO_2 loss during plant and microbial respiration were added to a land surface process model to simulate the diurnal and annual cycles of biosphere-atmosphere CO_2 exchange. The model was coupled to a modified version of the National Center for Atmospheric Research Community Climate Model version 2, and the coupled model was run for 5 years. The geographic patterns of annual net primary production are qualitatively similar to other models. When compared by vegetation type, annual production and annual microbial respiration are consistent with other models, except for needleleaf evergreen tree vegetation, where production is too high, and semidesert vegetation, where production and microbial respiration are too low. The seasonality of the net CO_2 flux agrees with other models in the southern hemisphere and the tropics. The diurnal range is large for photosynthesis and lower for plant and microbial respiration, which agrees with qualitative expectations. The simulation of the central United States is poor due to temperature and precipitation biases in the coupled model. Despite these deficiencies the current approach is a promising means to include terrestrial CO_2 fluxes in a climate system model that simulates atmospheric CO_2 concentrations, because it alleviates important parameterization discrepancies between standard biogeochemical models and the land surface models typically used in general circulation models, and because the model resolves the diurnal range of CO_2 exchange, which can be large (15–45 μmol CO_2 m^{-2} s^{-1}).

1. Introduction

Numerous models of land-atmosphere exchanges of energy, moisture, and momentum have been developed for use with atmospheric general circulation models (GCMs) (e.g., biosphere-atmosphere transfer scheme (BATS) [*Dickinson et al.*, 1993], simple biosphere model (SiB) [*Sellers et al.*, 1986], simple SiB [*Xue et al.*, 1991], bare essentials of surface transfer (BEST) [*Pitman et al.*, 1991], Canadian land surface scheme (CLASS) [*Verseghy*, 1991; *Verseghy et al.*, 1993], and schématisation des échanges hydriques à l'interface entre la biosphère et l'atmosphère (SECHIBA) [*Ducoudré et al.*, 1993]). These land surface process models provide the surface fluxes of solar radiation, infrared radiation, wind stresses, latent heat, and sensible heat required by GCMs, typically with a time step of less than 30 min.

Although land surface process models were originally conceived to account for differences among vegetation and soil types that affect biophysical land-atmosphere interactions, they may also provide a convenient means to add terrestrial CO_2 fluxes as part of a climate system model that simulates the diurnal and annual cycles of atmospheric CO_2 concentration. The physiological relationships between CO_2 assimilation and environmental factors such as air temperature, irradiance, vapor pressure, soil water, and foliage nitrogen are well understood. Models of terrestrial plant physiology that use these relationships to integrate daily or subdaily photosynthesis and respiration to annual net primary production (NPP) have shown that simple physiological assumptions provide reasonable simulations of seasonal and annual NPP over large climatic gradients [*Running and Coughlan*, 1988; *Running and Nemani*, 1988; *Bonan*, 1993b; *Foley*, 1994]. Moreover, the formulation of CO_2 fluxes in terms of canopy physiology and energy exchange resolves the discrepancies in temporal resolution and mechanistic detail between the simple parameterizations typically used in global models of terrestrial CO_2 exchange and the detailed parameterizations used in land surface models [*Bonan*, 1993c].

In this paper, I describe a terrestrial CO_2 flux parameterization for use with a land surface process model. The land surface model was coupled to an atmospheric general circulation model, and the coupled model was run for 5 years. The model is evaluated in terms of simulated net primary production, microbial respiration, and other CO_2 fluxes.

Paper number 94JD02961.
0148-0227/95/94JD-02961$05.00

2. Terrestrial CO_2 Fluxes

The land surface model (LSM version 0) solves for the canopy and ground temperatures that balance the surface energy budget (net radiation, sensible heat, latent heat, storage), taking into account ecological differences among vegetation types and hydraulic and thermal differences among soil types. In doing so, the model also calculates canopy absorption, reflection, and transmittance of solar radiation; snow and soil albedos; turbulent transfer; stomatal and soil resistances; interception and throughfall; snow

accumulation and melt; infiltration and runoff; and temperature and water for a six-layer soil. *Bonan* [1994] provides a thorough description of the biophysical components of the land surface model and comparisons with another land surface model. Here, I describe only the three terrestrial CO_2 fluxes: CO_2 uptake during photosynthesis, CO_2 loss during plant respiration, and CO_2 loss during microbial respiration.

Photosynthesis is coupled to the canopy conductance used for the latent heat flux. Canopy conductance is the average stomatal conductance for four leaves that differ in the amount of absorbed solar radiation. Leaf conductance is similar to that in the works by *Collatz et al.* [1991] and *Sellers et al.* [1992] and links stomatal conductance to photosynthesis as

$$g_{s,i} = mf(\psi)A_i \frac{P}{C_{s,i}} \frac{e_{s,i}}{e_*(T)} + g_{s,\min} \tag{1}$$

where $g_{s,i}$ is the stomatal conductance (μmol m^{-2} s^{-1}) for the ith leaf; m is a constant; A_i is foliage photosynthesis (μmol CO_2 m^{-2} s^{-1}); P is atmospheric pressure (pascals); $C_{s,i}$ is the CO_2 concentration at the leaf surface (pascals); $e_{s,i}$ is the vapor pressure at the leaf surface (pascals); $e_*(T)$ is the saturation vapor pressure (pascals) at the leaf temperature T; and $g_{s,\min}$ is the minimum stomatal conductance. The expression $f(\psi) = 1 - \exp[-c(\psi - \psi_c)]$ is a heuristic function that increases stomatal resistance as soil water decreases. The foliage water potential (megapascals) is $\psi = -0.01h - 0.2/f(\theta)$, where h is the average canopy height (meters) and $f(\theta)$ is the average ratio for the root zone of available soil water to maximum available soil water. This is not meant to be an exact parameterization of foliage water potential, but rather to mimic stomatal closure with dry soils.

Leaf photosynthesis is based on the works by *Farquhar et al.* [1980] and *Farquhar and von Caemmerer* [1982]. A_i is the minimum of the Rubisco limited rate of carboxylation

$$W_{c,i} = \frac{(C_{i,i} - \Gamma_*)V_m}{C_{i,i} + K_c(1 + O/K_o)} \tag{2}$$

and the ribulose bisphosphate regeneration-limited rate of carboxylation

$$W_{j,i} = \frac{(C_{i,i} - \Gamma_*)J_i}{4C_{i,i} + 8\Gamma_*} \tag{3}$$

where $C_{i,i}$ is the internal CO_2 concentration (pascals); $\Gamma_* = 0.105K_cK_o^{-1}O$ is the CO_2 compensation point (pascals); $K_c = K_{c25}a_{kc}^{(T-25)/10}$ and $K_o = K_{o25}a_{ko}^{(T-25)/10}$ are the Michaelis-Menten constants (pascals) for CO_2 and O_2, respectively, evaluated with foliage temperature T (degrees Celsius); $O = 0.209P$ is the internal O_2 concentration (pascals); $V_m = V_{m25}a_{vm}^{(T-25)/10}f(T)f(N)$ is the maximum rate of carboxylation (μmol CO_2 m^{-2} s^{-1}); and J_i is the potential electron transport (μmol electron m^{-2} s^{-1}). J_i is the smaller of the roots that satisfy

$$0.7J_i^2 - (J_m + 0.38\Phi_i)J_i + 0.38J_m\Phi_i = 0 \tag{4}$$

where $J_m = J_{m25}a_{jm}^{(T-25)/10}f(T)f(N)$ is the maximum electron transport (μmol electron m^{-2} s^{-1}); and Φ_i is the absorbed photosynthetically active radiation (μmol photon m^{-2} s^{-1}). Here $f(N) = N/N_m$ is a function that adjusts the rate of photosynthesis for foliage nitrogen (N), and $f(T)$ is a function that mimics thermal breakdown of metabolic processes:

$$f(T) = \left\{1 + \exp\left[\frac{-220{,}000 + 710(T + 273)}{8.314(T + 273)}\right]\right\}^{-1}. \tag{5}$$

$A_i = 0$ when the canopy air temperature is less than $T_{\min}$. *Bonan* [1993a] provides further details on implementing the photosynthesis submodel.

$C_{i,i}$, $C_{s,i}$, and $e_{s,i}$ are calculated as

$$C_{i,i} = C_a - PA_i\left(\frac{1.37}{g_b} + \frac{1.65}{g_{s,i}}\right)$$

$$C_{s,i} = C_a - \frac{1.37}{g_b}PA_i \tag{6}$$

$$e_{s,i} = \left[\frac{e_a}{g_{s,i}} + \frac{e_*(T)}{g_b}\right] \Bigg/ \left[\frac{1}{g_{s,i}} + \frac{1}{g_b}\right]$$

where $C_a = 340 \times 10^{-6}P$ is the ambient CO_2 concentration (pascals); g_b is the leaf boundary layer conductance (μmol m^{-2} s^{-1}); and e_a is the vapor pressure of canopy air (pascals).

Respiration is broken into maintenance respiration, which depends on temperature, and growth respiration, which is temperature independent. Maintenance respiration R_m (μmol CO_2 m^{-2} s^{-1}) is

$$R_m = LR_{f25}(1 + p)a_r^{(T-25)/10} \tag{7}$$

where L is the total leaf area index; R_{f25} is foliage respiration at 25°C (μmol CO_2 m^{-2} s^{-1}); and $a_r = 2.0$ is the temperature sensitivity parameter. Rather than explicity accounting for stem sapwood and root respiration as the product of a rate per unit biomass and biomass per unit area [e.g., *Bonan*, 1993a, b], the parameter p is the contribution to total maintenance respiration by nonfoliage plant material. Respiration is reduced by one half outside of the growing season [cf. *Bonan*, 1991]. Growth respiration R_g (μmol CO_2 m^{-2} s^{-1}) is

$$R_g = \kappa A_c \tag{8}$$

where $\kappa = 0.25$ [*Jones*, 1992] and $A_c = \sum A_iL_i$ is the total canopy photosynthesis summed over the four layers.

Net primary production (micrograms per square meter) is

$$\Delta M = \gamma(A_c - R_m - R_g)\Delta t \tag{9}$$

where $\gamma = 28.5$ μg μmol^{-1} CO_2 [*Landsberg*, 1986] and $\Delta t = 1200$ is the time step (seconds).

As in the work by *Bonan* [1991], microbial respiration R_s (μmol CO_2 m^{-2} s^{-1}) is based on the work of *Bunnell et al.* [1977]:

$$R_s = \frac{\theta}{a_1 + \theta}\frac{a_2}{a_2 + \theta}a_3a_4^{(T_{s,1}-10)/10} \tag{10}$$

where a_1 is one-half field capacity; a_2 is one-half saturation; a_3 is the optimal respiration rate at 10°C (i.e., the product of the respiration rate per unit biomass and the soil carbon per

Table 1. Land Surface Model (LSM) Land Surface Types

	Plant Types and Fractional Area					
	Type 1	Area 1	Type 2	Area 2	Type 3	Area 3
Land ice	B	1.00				
Desert	B	1.00				
Needleleaf evergreen forest	NET	0.75	B	0.25		
Needleleaf deciduous forest	NDT	0.50	B	0.50		
Broadleaf deciduous forest	BDT	0.75	B	0.25		
Mixed	NET	0.37	BDT	0.37	B	0.26
Broadleaf evergreen forest	BET	0.95	B	0.05		
Savanna	G	0.70	TDT	0.30		
Evergreen forest tundra	NET	0.50	AG	0.25	B	0.25
Deciduous forest tundra	NDT	0.50	AG	0.25	B	0.25
Forest crop	C	0.60	BDT	0.25	B	0.15
Grassland	G	0.80	B	0.20		
Tundra	ADS	0.30	AG	0.30	B	0.40
Evergreen shrubland	ES	0.80	B	0.20		
Deciduous shrubland	DS	0.80	B	0.20		
Semidesert	DS	0.10	B	0.90		
Crop	C	0.85	B	0.15		
Forest wetland	BET	0.80	B	0.20		
Nonforest wetland	B	1.00				

Each surface type is composed of multiple plant types and bare ground (B). NET, needleleaf evergreen tree; NDT, needleleaf deciduous tree; BET, broadleaf evergreen tree; BDT, broadleaf deciduous tree; TDT, tropical deciduous tree; G, grass; ES, evergreen shrub; DS, deciduous shrub; ADS, arctic deciduous shrub; AG, arctic grass; C, crop.

unit area); a_4 is a temperature sensitivity parameter; θ is the average soil water content for the root zone; and $T_{s,1}$ is the temperature of the first soil layer (i.e., at a depth of 5 cm). A typical value used in global models is $a_4 = 2.0$ [*Raich et al.*, 1991; *Raich and Schlesinger*, 1992; *Potter et al.*, 1993]. Values of $a_1 = 0.20$ and $a_2 = 0.23$ are typical of loamy soil.

3. Coupled Land-Atmosphere Model

The atmospheric model is a modified version of the National Center for Atmospheric Research Community Climate Model version 2 (CCM2). Model physics and dynamics have been described by *Hack et al.* [1993]. *Hack et al.* [1994] discuss the climatology of the model, and *Kiehl et al.* [1994] describe the Earth radiation budget simulation of the model. Briefly, CCM2 is a spectral general circulation model configured at T42 resolution (approximately 2.8° × 2.8° transform grid). The model has 18 vertical levels with the model top at 2.9 mbar. The standard model uses prescribed climatologically varying sea surface temperatures, prescribed surface albedos, and prescribed surface wetness. The model has a 20-min time step, but atmospheric radiation calculations are only performed every model hour. For the current simulations the model has been modified to distinguish between continental and maritime cloud drop effective radius, as discussed by *Kiehl* [1994]. The liquid water scale height is a function of total precipitable water (J. J. Hack, unpublished research, 1994). In coupling with the land surface model, the land surface model provides to the atmospheric model sensible heat flux, latent heat flux, water vapor flux, radiative temperature, albedos, surface stresses, 2-m-height air temperature, and 2-m-height specific humidity. The atmospheric model provides to the land model solar radiation fluxes, downward longwave radiation, total precipitation, and lowest model level air temperature, wind speeds, specific humidity, pressure, and height.

The land surface model is implemented with the assumption that major vegetation types (e.g., tundra, forest tundra, grassland, etc.) are composed of bare ground and several functional plant types that differ in physiology and other important characteristics (Table 1). Rather than having the model use a blended surface type for each CCM2 land point (e.g., as in BATS, SiB, BEST), the model performs separate calculations for each subtype, treating each subarea independently. In this respect, the land surface model is similar to CLASS and SECHIBA. Each subgrid area receives the same atmospheric forcing, and grid-averaged fluxes passed back to the atmosphere are obtained by weighting the fluxes for each subgrid area by the fractional areas. Surface types were derived from *Olson et al.*'s [1983] 0.5° × 0.5° data set. Each CCM2 land point also has a lake fraction, for which the land surface model calculates the surface energy budget of a lake. Lake temperatures are updated using a one-dimensional thermal stratification model based on eddy diffusion concepts. In its T42 configuration, the atmospheric model has 2749 land points; there are 5623 LSM points.

Physiological parameters that do not vary among vegeta-

Table 2. Stomatal Resistance Parameters

Parameter	Value
a_{vm}	2.4
c, MPa^{-1}	0.5
J_{m25}, $\mu mol\ m^{-2}\ s^{-1}$	100
a_{jm}	1.7
K_{c25}, Pa	30
a_{kc}	2.1
K_{o25}, Pa	30,000
a_{ko}	1.2
m	9
N_m, %	1.5
$g_{s,min}$, $\mu mol\ m^{-2}\ s^{-1}$	2,000
ψ_c, MPa	−2.0

These parameters do not vary among plant types.

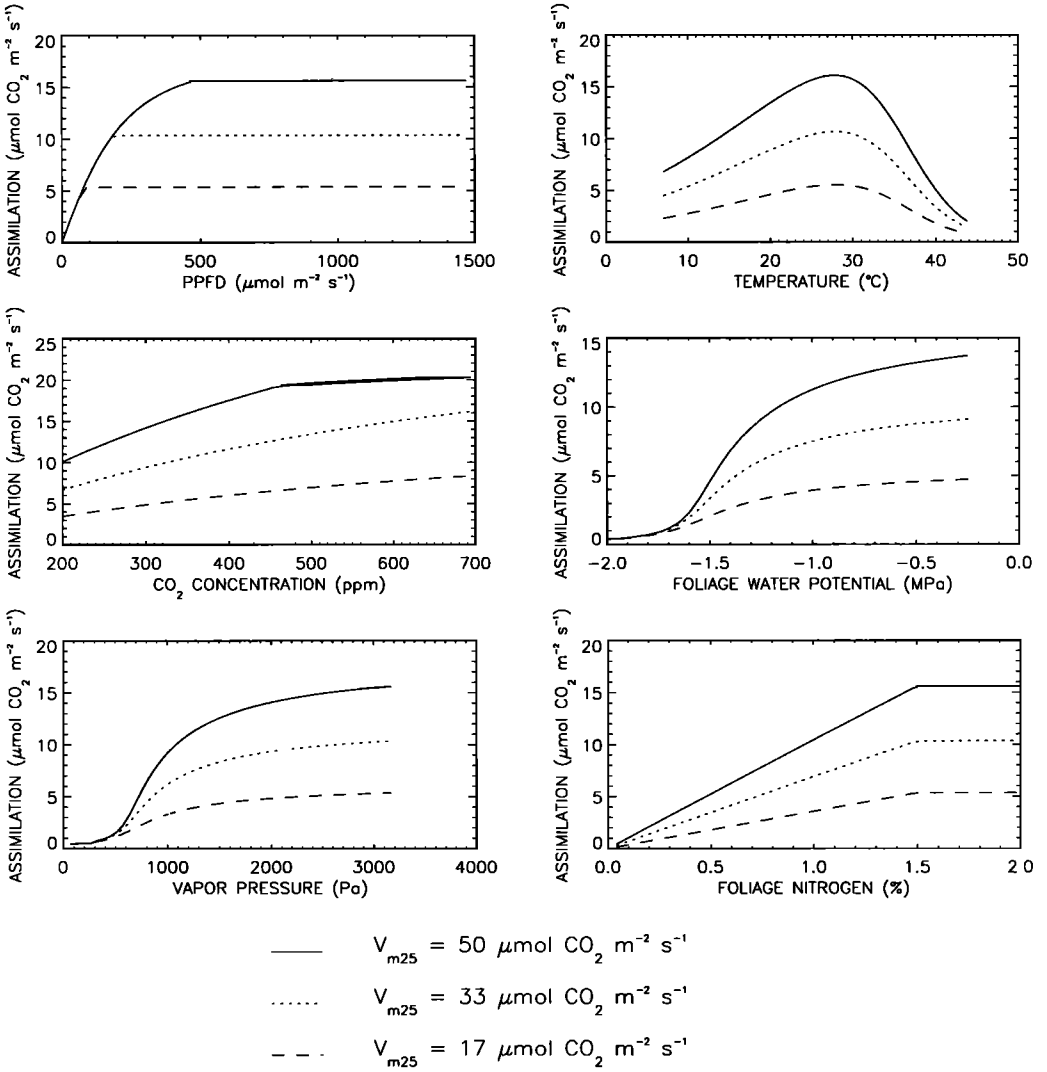

Figure 1. Photosynthetic response to photosynthetic photon flux (PPFD), temperature, atmospheric CO_2 concentration, foliage water potential, vapor pressure, and foliage nitrogen for three values of V_{m25}.

tion types are listed in Table 2. K_{c25}, K_{o25}, a_{kc}, a_{ko}, a_{vm}, and m are from *Collatz et al.* [1991] and *Sellers et al.* [1992]. The parameters ψ_c and c are heuristic parameters that ensure reasonable stomatal closure with dry soils. The value of $g_{s,\min}$ was chosen to give a maximum stomatal resistance of 20,000 s m^{-1}. J_{m25} and a_{jm} are from *Bonan* [1993a, b]. Figures 1 and 2 illustrate photosynthetic and stomatal responses to various environmental factors.

Table 3. LSM Plant Types and Parameters

Plant	z_0, m	d, m	d_L, m	V_{m25}, μmol CO_2 m^{-2} s^{-1}	R_{f25}, μmol CO_2 m^{-2} s^{-1}	p	$T_{\min}$, °C	a_3, μmol CO_2 m^{-2} s^{-1}
NET	0.94	11.39	0.04	33	0.50	0.4	−5	4.1
NDT	0.77	9.38	0.04	33	0.50	0.4	−5	4.1
BET	2.62	23.45	0.04	50	0.75	0.4	5	3.5
BDT	1.10	13.40	0.04	33	0.50	0.4	0	4.4
TDT	0.99	12.06	0.04	50	0.75	0.4	5	1.0
G	0.06	0.34	0.04	33	0.50	0.0	0	1.7
ES	0.06	0.34	0.04	17	0.26	0.0	−5	2.1
DS	0.06	0.34	0.04	17	0.26	0.0	0	2.1
ADS	0.06	0.34	0.04	33	0.50	2.6	0	1.7
AG	0.06	0.34	0.04	33	0.50	2.6	0	1.7
C	0.06	0.34	0.04	50	0.75	0.0	0	2.5

Plant abbreviations are as in Table 1. Parameters are as follows: z_0, roughness length; d, displacement height; d_L, leaf dimension; V_{m25}, maximum carboxylation at 25°C; R_{f25}, foliage respiration at 25°C; p, nonfoliage contribution to maintenance respiration; $T_{\min}$, minimum temperature for photosynthesis; and a_3, microbial respiration parameter.

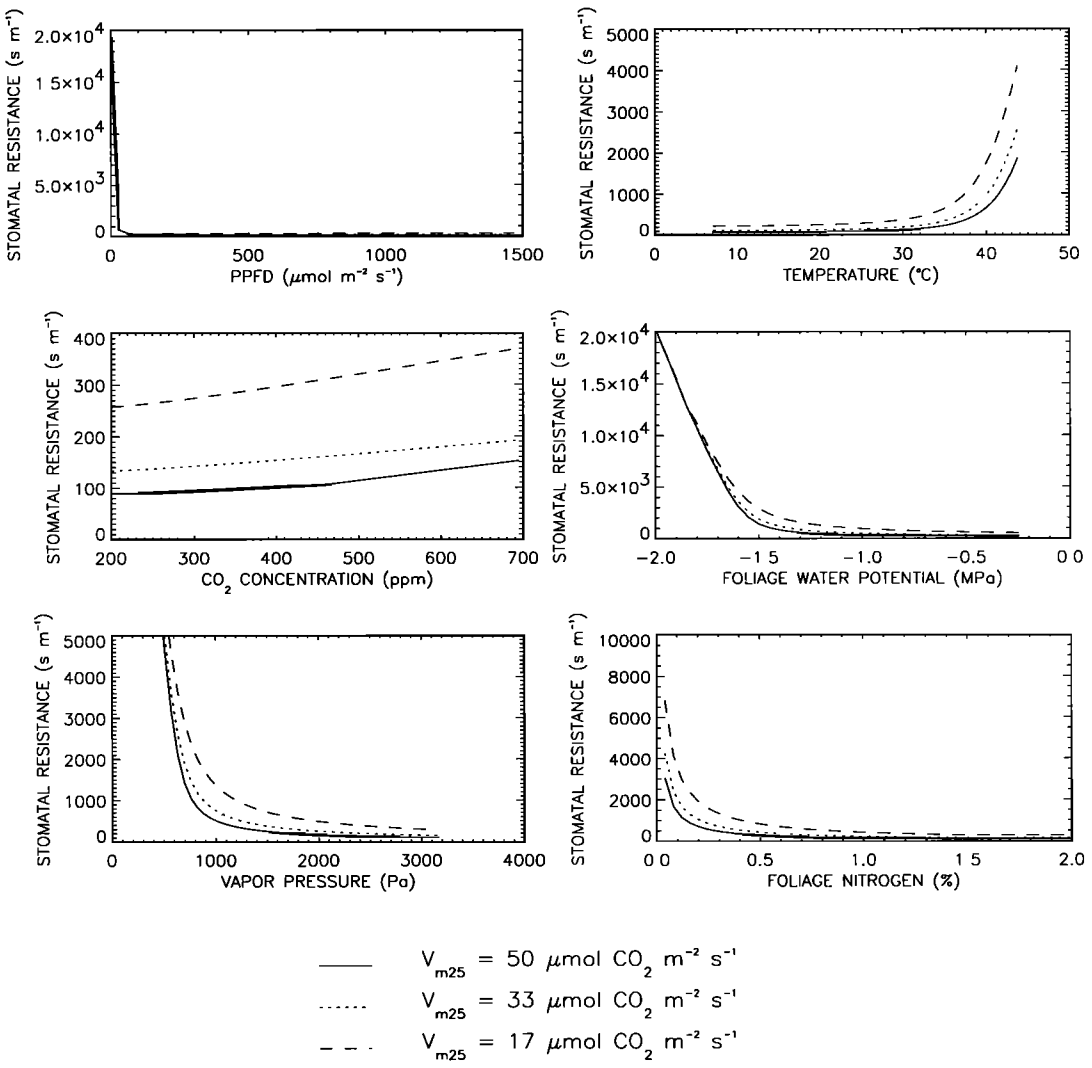

Figure 2. As in Figure 1 but for stomatal resistance.

Table 4. Hydraulic and Thermal Properties for Coarse-, Intermediate-, and Fine-Grain Soils

	Coarse	Intermediate	Fine
$k_{h,sat}$, mm s^{-1}	0.0347	0.0070	0.0013
b	4.90	5.39	11.40
ψ_{sat}, mm	−218	−478	−405
θ_{sat}, m^3 m^{-3}	0.435	0.451	0.482
θ_{dry}, m^3 m^{-3}	0.113	0.154	0.286
c_{sol}, MJ m^{-3} °K^{-1}	2.18	2.26	2.33
$k_{t,sol}$, W m^{-1} °K^{-1}	7.6	5.8	4.1

Hydraulic properties are from *Clapp and Hornberger* [1978]. Thermal properties are from data for quartz and clay minerals given by *Monteith and Unsworth* [1990], assuming coarse soil is 80% quartz, 20% clay mineral; intermediate soil is 50% quartz, 50% clay mineral; and fine soil is 80% clay mineral, 20% quartz. Parameters are as follows: $k_{h,sat}$, saturated hydraulic conductivity; b, Clapp and Hornberger parameter; ψ_{sat}, soil matrix potential at saturation; θ_{sat}, soil water content at saturation (porosity); θ_{dry}, soil water content when transpiration stops; c_{sol}, heat capacity of soil solids; $k_{t,sol}$, thermal conductivity of soil solids.

Leaf and stem reflectance and transmittance, leaf orientation, and canopy height vary among vegetation types as in the work by *Dorman and Sellers* [1989]. Monthly leaf and stem area for each vegetation type were also taken from *Dorman and Sellers* [1989]. Other parameters that vary with vegetation type are listed in Table 3. The roughness length and displacement heights were chosen so that the neutral drag coefficient is consistent with values used in CCM2 and BATS. The leaf dimension is from BATS. V_{m25} was chosen to give maximum photosynthetic rates of approximately 5, 10, and 15 μmol m^{-2} s^{-1} in the light response curves (Figure 1). These values are consistent with values reported by *Woodward and Smith* [1994] and were assigned to vegetation types based on their data. R_{f25} is 1.5% of V_{m25} [*Farquhar et al.*, 1980; *Collatz et al.*, 1991; *Sellers et al.*, 1992]. T_{min} are reasonable values of when plants photosynthesize with respect to temperature. For these simulations, $f(N) = 1$. Values for a_3 and p were chosen based on "off-line" simulations. The land surface model was forced with mean

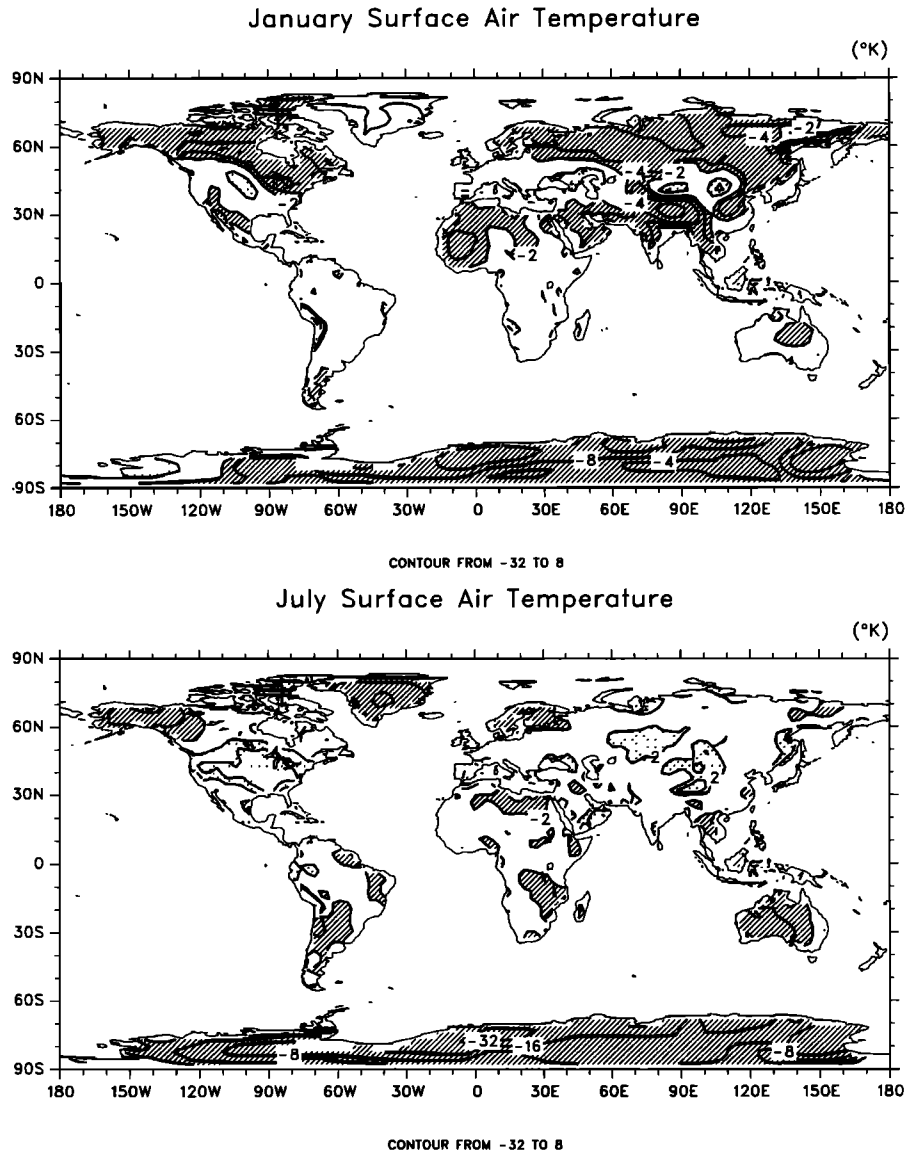

Figure 3. Simulated minus observed 2-m-height air temperature for January and July. Contour intervals are 0°, ±2°, ±4°, ±8°, −16°, and −32°C. Areas greater than 2°C are stippled and less than −2°C are hatched. Simulated data are averaged over the 5-year simulation. Observed data are from *Legates and Willmott* [1990a].

monthly climatological data for 118 sites in the United States and Canada [*Bryson and Hare*, 1974], 12 sites in Mexico [*Bryson and Hare*, 1974], 8 sites in Siberia [*Lydolph*, 1977], and 17 sites in South America [*Schwerdtfeger*, 1976]. Monthly data were interpolated to daily data and then to 20-min data. Values of a_3 and p were chosen so that annual microbial respiration and annual net primary production were consistent with observations (see *Raich and Schlesinger* [1992] and *Melillo et al.* [1993], respectively). This type of calibration is common in global models of terrestrial carbon fluxes [*Raich et al.*, 1991; *McGuire et al.*, 1992; *Potter et al.*, 1993]. For trees, p varied only slightly and p = 0.40 was chosen as a common value.

Soil hydraulic and thermal properties vary with coarse-, intermediate-, and fine-grained texture types (Table 4). The soil texture data set used for the current simulations was derived from the BATS T42 data set [*Dickinson et al.*, 1993]. Soils for irrigated crops are kept wet during the growing season. As in BATS, a soil color data set is required for the soil albedo calculation, and the BATS T42 data set was used for the current simulation.

4. Simulated CO_2 Fluxes

The coupled land-atmosphere model has some biases that are important when evaluating the CO_2 fluxes. The model has extensive regions of colder (4°–8°C) than observed surface air temperatures for snow-covered regions in January (Figure 3). This results, in part, from too high snow albedos. Although much of the land is within ±2°C of observations in July, central North America shows a large warm bias (4°–8°C). The July warm temperature bias is a persistent feature of the CCM2 and subsequent versions of the model, even without the interactive land surface model

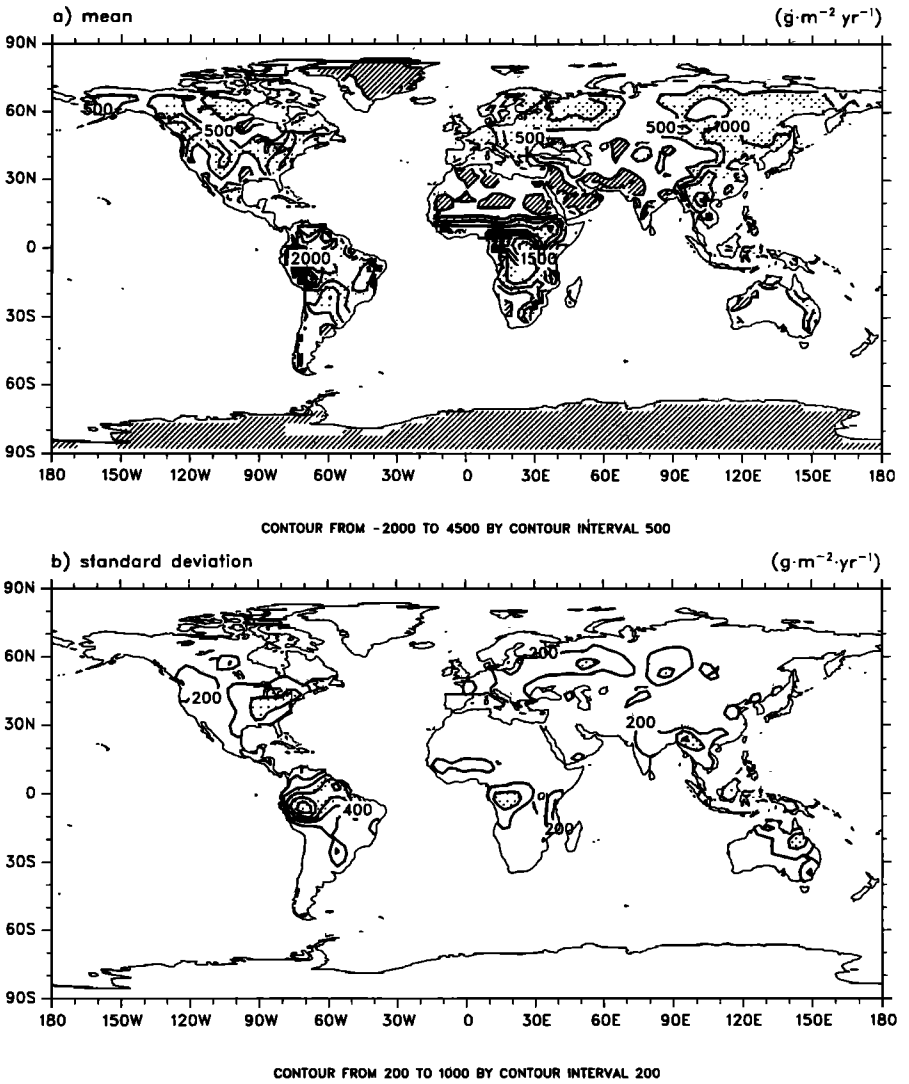

Figure 4. Annual net primary production. (a) Five-year mean. Stippling shows areas >500 g m^{-2} yr^{-1}. Hatching indicates NPP < 0. (b) Standard deviation. Stippling shows areas >400 g m^{-2} yr^{-1}.

Table 5. Average Annual Net Primary Production (NPP)

Vegetation Type	This Study	Lieth	Potter et al.	Melillo et al.
Needleleaf evergreen forest	1,018	680	452	551
Needleleaf deciduous forest	478	363	306	...
Broadleaf deciduous forest	865	1,541	630	1,525
Mixed forest	676	772	632	1,338
Broadleaf evergreen forest	2,422	2,246	2,054	2,085
Savanna	1,392	1,589	1,118	752
Forest tundra	747	354	...	346
Grassland	596	863	360	533
Tundra	286	342	160	240
Shrubland	228	911	368	296
Semidesert	8	329	56	106
Crop	874	...	576	...

Values are in grams per square meters per year. Lieth, derived from observed air temperature and precipitation [*Legates and Willmott*, 1990a, b] using empirical relationships between net primary production and mean annual air temperature and annual precipitation [*Lieth*, 1975]. Potter et al., from Table 7 of *Potter et al.* [1993], assuming biomass is 50% carbon. Melillo et al., from Table 2 of *Melillo et al.* [1993], assuming biomass is 50% carbon.

Table 6. Average Annual CO_2 Fluxes

Vegetation Type	Photosynthesis	Plant Respiration	Microbial Respiration	Net Flux
Needleleaf evergreen forest	3,696	2,123	671	−901
Needleleaf deciduous forest	1,215	477	382	−357
Broadleaf deciduous forest	3,028	1,693	1,697	361
Mixed forest	2,635	1,591	784	−260
Broadleaf evergreen forest	12,984	9,244	2,870	−870
Savanna	4,383	2,234	1,720	−429
Forest tundra	2,181	1,028	354	−799
Grassland	2,150	1,230	1,098	179
Tundra	1,020	579	164	−278
Shrubland	752	400	1,795	1,443
Semidesert	31	18	222	210
Crop	2,904	1,555	1,510	161

Values are in grams per square meter per year. Net flux equals plant respiration plus microbial respiration minus photosynthesis.

[*Hack et al.*, 1994]. With an interactive land, soils in this region dry out during the summer, reducing the latent heat flux.

Net Primary Production (NPP)

Highest annual production occurs in equatorial regions of South America and Africa, southeast Asia, eastern North America, and Europe (Figure 4a). These patterns are qualitatively similar to global NPP maps produced by *Melillo et al.* [1993], *Potter et al.* [1993], and *Foley* [1994]. One important exception from these maps is the low NPP in much of the central United States. This is caused by low summer soil water due to the large warm temperature bias in July (Figure 3) and less than observed precipitation in January and July. NPP has large interannual variability, with standard deviations greater than 200 g m^{-2} yr^{-1} in the regions of high production (Figure 4b).

NPP is summarized by vegetation type in Table 5. The most striking feature is the wide range in NPP among the Lieth, Potter et al., and Melillo et al. estimates. For example, mixed forest NPP ranges from 632 to 772 g m^{-2} yr^{-1} in Lieth and Potter et al., but is 1338 g m^{-2} yr^{-1} in Melillo et al. Similar discrepancies can be found in most vegetation types. Broadleaf evergreen forest is the only vegetation type that showed reasonable consistency. The NPP simulated in this study is within the range of the other estimates with three exceptions: NPP is too high in needleleaf evergreen forest and forest tundra, and NPP is too low in semidesert. For semidesert, this is due to the low fractional area of vegetation (10%) and low photosynthetic rates (Table 6). For the other types the high NPP is due to high canopy photosynthetic rates arising from high leaf area index (e.g., needleleaf evergreen trees have a leaf area index >7 during the growing season).

In Figure 5, simulated annual NPP is compared on a grid point basis to estimates obtained using *Legates and Willmott*'s [1990a, b] temperature and precipitation data and *Lieth*'s [1975] empirical equations. A linear regression between the two estimates shows a significant positive relationship. The intercept is not significantly different from zero, but the slope is significantly less than one. *Foley* [1994] provided a similar comparison of his NPP estimates with those from *Lieth*'s [1975] equations. His NPP shows much less scatter, perhaps because he calculated NPP based on observed rather than simulated climatology. The NPP simulated in this study is negative for numerous grid points (Figure 5). The negative NPP occurs primarily in semidesert regions and the south central United States (Figure 4).

The seasonality of the model is illustrated with mean monthly fluxes for January and July. Photosynthetic rates clearly show the "greening up" of the land. In January, high rates of photosynthesis occur in tropical latitudes and the southern hemisphere; much of the northern hemisphere is dormant or has rates less than 2 μmol CO_2 m^{-2} s^{-1} (Figure 6a). However, during July the northern hemisphere shows considerable photosynthetic activity (Figure 6b). Central North America is the noticeable exception. Plant respiration has a seasonal pattern similar to photosynthesis (Figure 7).

The diurnal cycle of the model is illustrated by the diurnal range in CO_2 fluxes for January 17 and July 17 of the third year (Table 7). During the growing season, photosynthesis has the largest diurnal range, greater than 25 μmol CO_2 m^{-2} s^{-1} in tropical vegetation. Other vegetation types have ranges from 6 to 12 μmol CO_2 m^{-2} s^{-1} in the growing season. Plant respiration has a lower diurnal range, generally

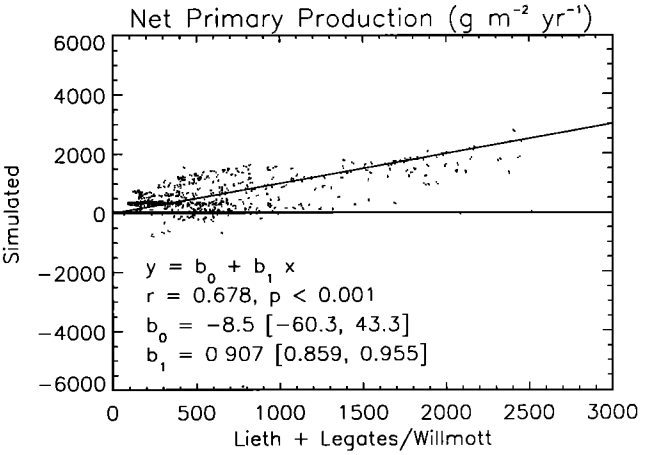

Figure 5. NPP simulated by this study compared to NPP obtained using *Legates and Willmott*'s [1990a, b] climatology and *Lieth*'s [1975] empirical relationships with mean annual air temperature and annual precipitation. Data are for 1620 model grid points, excluding land ice, forest crop, and crop surface types. The Legates and Willmott climatology was mapped to the 2.8° × 2.8° horizontal grid used by the model. Numbers in brackets are the 95% confidence interval for b_0 and b_1.

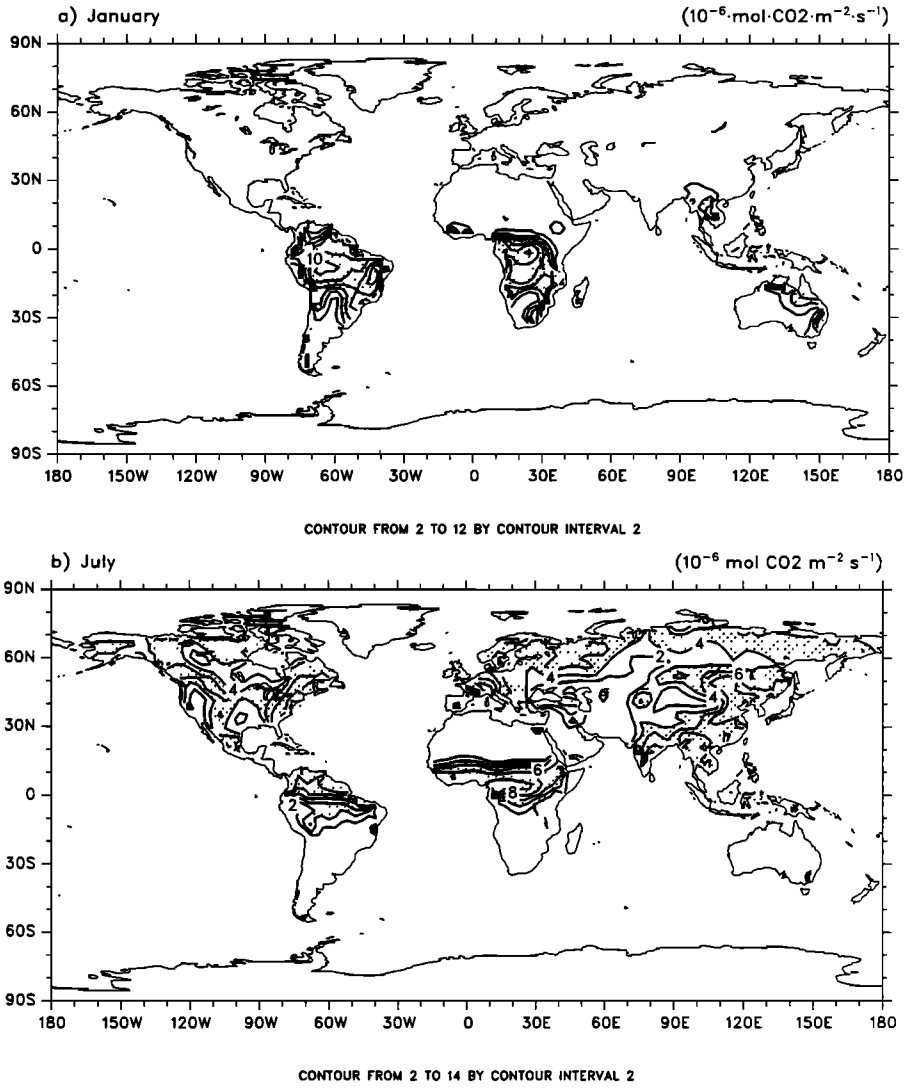

Figure 6. (a) January and (b) July photosynthesis. Stippling shows areas >4 μmol CO_2 m^{-2} s^{-1}.

less than 10 μmol CO_2 m^{-2} s^{-1} (one-half to one-third the range of photosynthesis). The large diurnal range in photosynthesis is due to high uptake during the day, when the irradiance is high, and no uptake at night. In contrast, respiration depends primarily on temperature and has less of a diurnal cycle.

Microbial Respiration

Annual microbial respiration is highest in equatorial regions and in the south central United States (Figure 8a). The standard deviation is typically <10% of the 5-year mean (Figure 8b). Mean annual microbial respiration for certain vegetation types is fairly consistent with observations (Table 8). Most vegetation types have a mean well within ± 1 standard deviation of observations. The one exception is semidesert, which is two standard deviations less than the observed values. Microbial respiration has a geographic dependent seasonality: tropical regions have high fluxes throughout the year, while extratropical regions have high fluxes only in the warm months (Figure 9). During the growing season the diurnal range in microbial respiration (<1 μmol CO_2 m^{-2} s^{-1}) is more than 10 times less than that of photosynthesis (Table 7).

Annual Net CO_2 Flux

The validity of annual net CO_2 flux, the difference between CO_2 uptake during plant production and CO_2 loss during microbial respiration, depends on the validity of simulated NPP and microbial respiration. Much of the world is an annual source of CO_2 to the atmosphere (Figure 10a). The large annual source of CO_2 in central North America clearly is a spurious result of the climatological biases, resulting in low NPP in this region. Needleleaf evergreen forest has the greatest CO_2 uptake per unit area due to high rates of NPP and low microbial respiration (Table 6). On average, broadleaf evergreen forest is a net CO_2 sink (Table 6), but this varies geographically with equatorial Africa being a source (Figure 10a).

In central North America, Europe, southeast Asia, and equatorial South America and Africa, net CO_2 has large interannual variability, with standard deviations >400 g CO_2

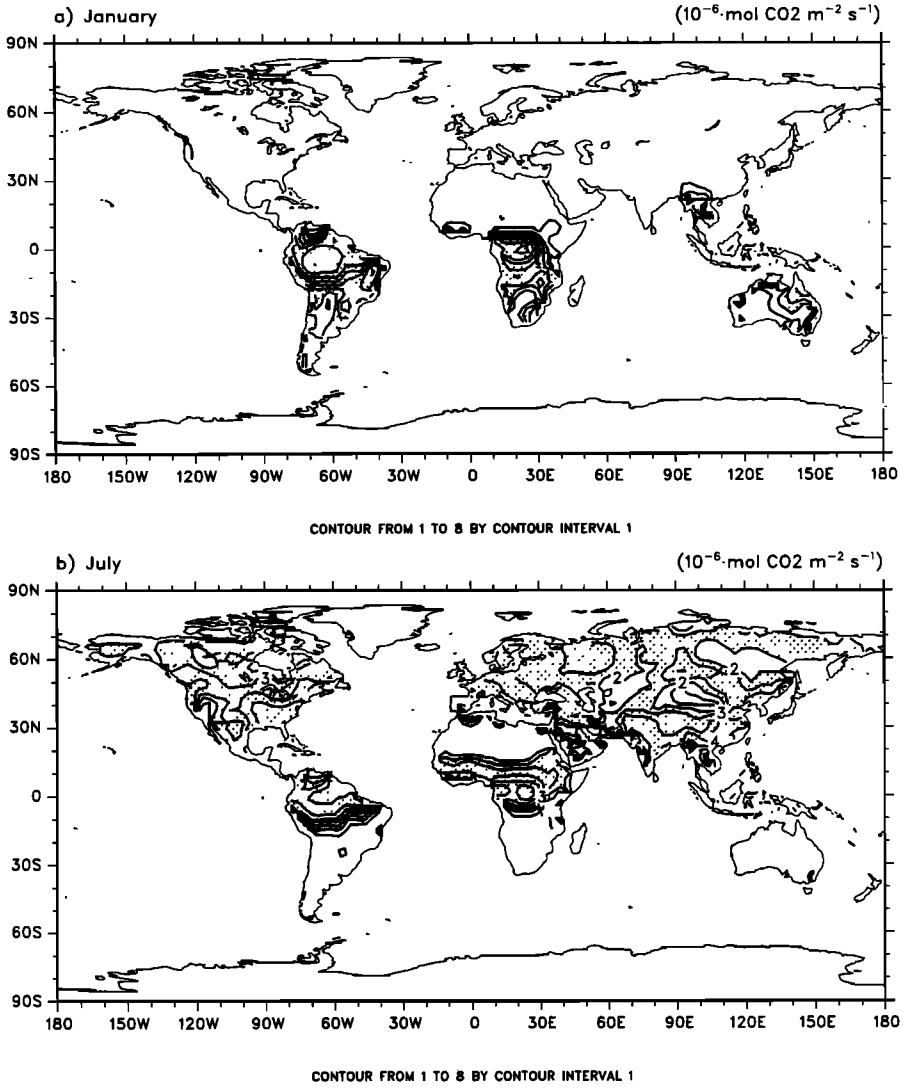

Figure 7. (a) January and (b) July plant respiration. Stippling shows areas >2 μmol CO_2 m^{-2} s^{-1}.

m^{-2} yr^{-1} (Figure 10b). These values reflect the high sensitivity of the model to changes in temperature and precipitation.

During January, much of the land is a source of CO_2 to the atmosphere (Figure 11a). Only tropical regions and some areas of the southern hemisphere are large net CO_2 sinks, due to the high rates of photosynthesis. In July, however, much of the southern hemisphere is a source of CO_2 (Figure 11b). A narrow band around the equator is still a large CO_2 sink. Most of the northern hemisphere is a CO_2 sink, with the exception of desert and grassland areas of central Asia and central North America. In the southern hemisphere and in the tropics, the seasonality of the net flux agrees with the

Table 7. Average Diurnal Range for January 17 and July 17 of the Third Year

	January			July		
Vegetation Type	P	R_p	R_m	P	R_p	R_m
Needleleaf evergreen forest	1.5	0.5	0.0	10.8	5.3	0.7
Needleleaf deciduous forest	0.0	0.0	0.0	6.0	2.2	0.5
Broadleaf deciduous forest	2.2	0.6	0.3	12.3	4.7	0.8
Mixed forest	1.0	0.3	0.1	8.8	4.4	0.7
Broadleaf evergreen forest	25.6	10.5	0.8	27.4	10.6	0.8
Savanna	12.3	4.0	1.0	12.7	4.1	0.7
Forest tundra	0.1	0.0	0.0	10.4	3.5	0.2
Grassland	4.4	1.8	0.5	8.7	5.6	0.9
Tundra	0.1	0.4	0.0	6.4	3.2	0.2

P, photosynthesis (μmol CO_2 m^{-2} s^{-1}); R_p, plant respiration (μmol CO_2 m^{-2} s^{-1}); R_m, microbial respiration (μmol CO_2 m^{-2} s^{-1}).

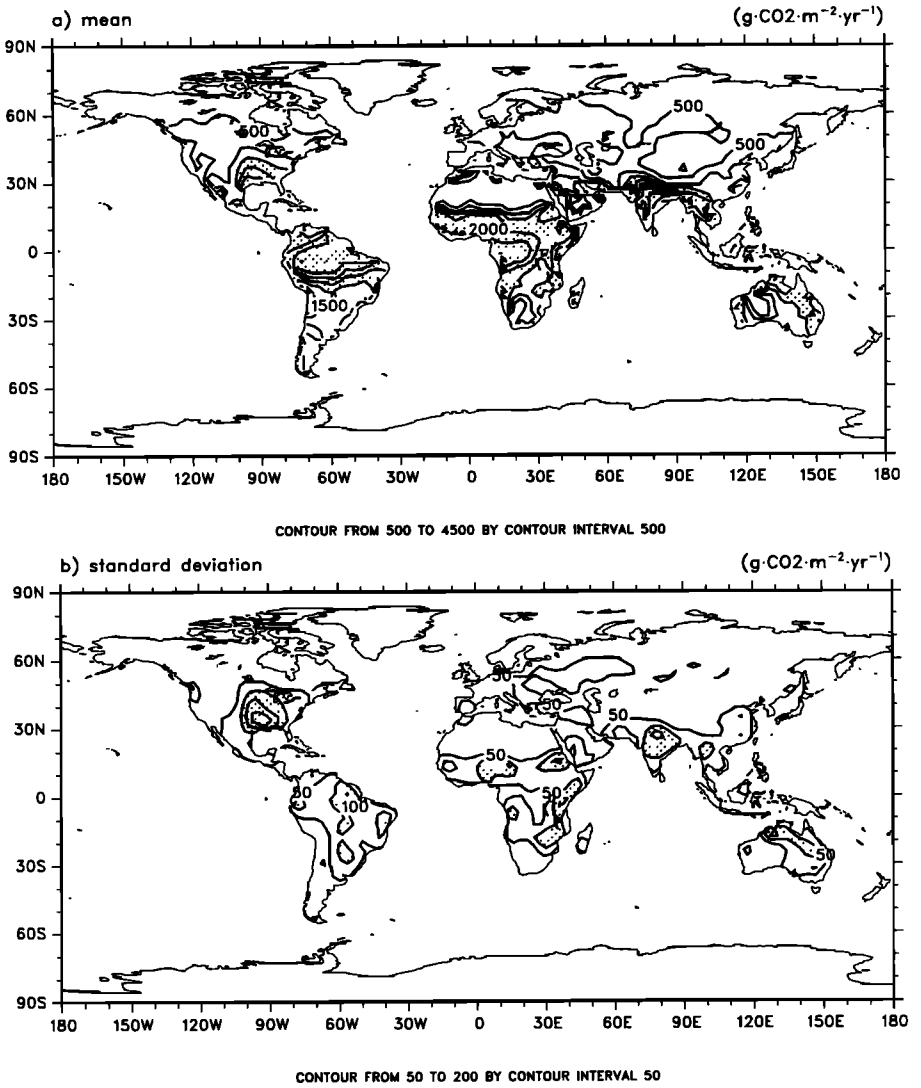

Figure 8. Annual microbial respiration. (a) Five-year mean. Stippling shows areas >1500 g CO_2 m^{-2} yr^{-1}. (b) Standard deviation. Stippling shows areas >100 g m^{-2} yr^{-1}.

Table 8. Simulated and Observed Annual Microbial Respiration

Simulated		Observed	
Vegetation Type	Mean, g CO_2 m^{-2} yr^{-1}	Vegetation Type	Mean ± s.d., g CO_2 m^{-2} yr^{-1}
Tundra	164	tundra	154 ± 51
Needleleaf forest	593	boreal forest	826 ± 318
Grassland	1,098	grassland	1,134 ± 600
Broadleaf deciduous and mixed forest	1,065	temperate forest	1,661 ± 705
Shrubland	1,795	shrubland	1,830 ± 814
Cropland	1,510	cropland	1,396 ± 1047
Semidesert	222	desert scrub	575 ± 169
Savanna	1,720	savanna	1,614 ± 408
Broadleaf evergreen forest	2,870	tropical moist forest	3,234 ± 463

Observed data are from Table 1 of *Raich and Schlesinger* [1992], assuming 30% of soil respiration is from roots (i.e., as in their Table 3). Here s.d. denotes standard deviation.

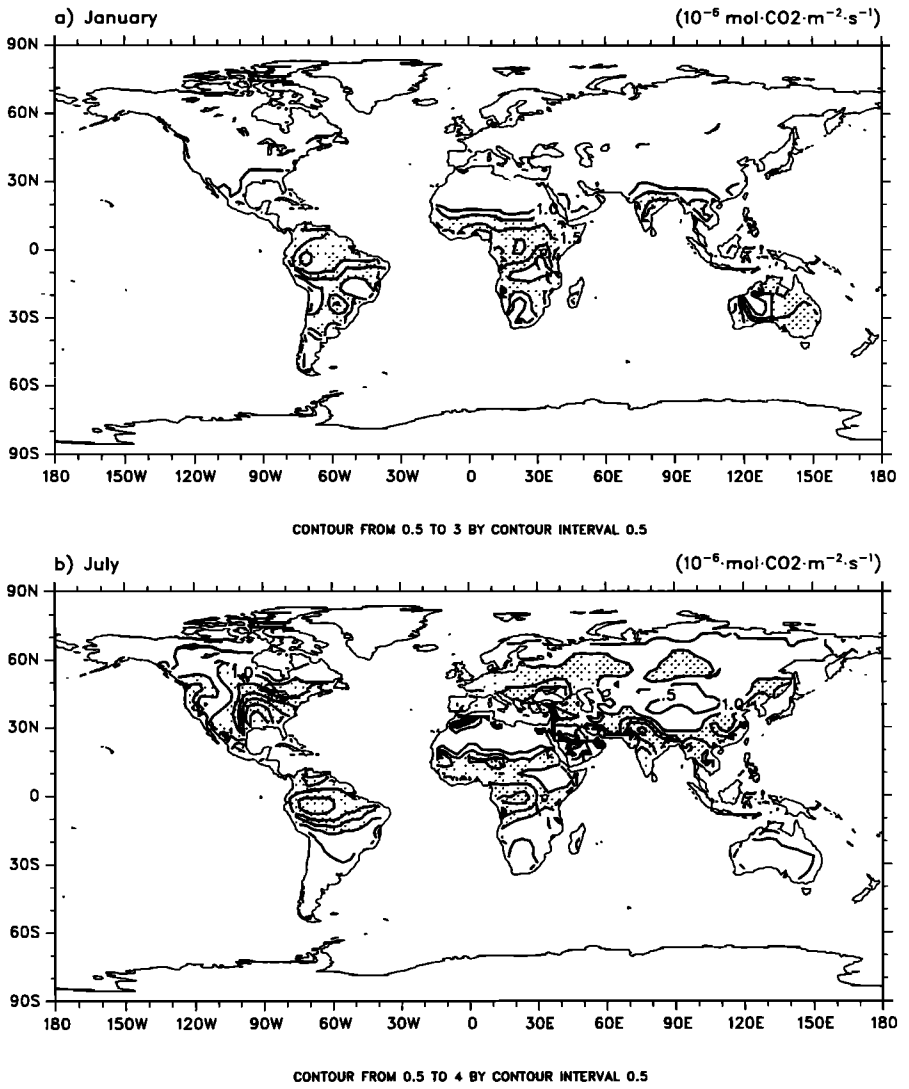

Figure 9. (a) January and (b) July microbial respiration. Stippling shows areas >1 μmol CO_2 m^{-2} s^{-1}.

simulations of *Potter et al.* [1993, Plate 3a]. However, the northern hemisphere July is inconsistent due to the high (2–8 μmol CO_2 m^{-2} s^{-1}) efflux in central North America.

5. Discussion

Simulations with a coupled land-atmosphere model showed that CO_2 fluxes can be successfully added to a land surface process model to simulate the diurnal and annual cycles of biosphere-atmosphere CO_2 exchange. The geographic patterns of annual NPP are qualitatively similar to other models [*Melillo et al.*, 1993; *Potter et al.*, 1993; *Foley*, 1994], with highest annual production in equatorial regions of South America and Africa, southeast Asia, eastern North America, and Europe. When compared by vegetation type, annual NPP and annual microbial respiration are consistent with other estimates, except for needleleaf evergreen tree vegetation, where NPP is too high, and semidesert vegetation, where NPP and microbial respiration are too low. The seasonality of the net CO_2 flux agrees with other simulations in the southern hemisphere and the tropics. The diurnal range is large for photosynthesis and lower for plant and microbial respiration, which agrees with qualitative expectations.

One recurring problem with the model is the poor simulation in the central United States, where NPP is too low, the model predicts an annual net flux of CO_2 to the atmosphere, and the seasonality is inconsistent with other studies due to high CO_2 efflux in July. These problems reflect temperature and precipitation biases in the coupled model and cannot be corrected without changing the physics of the land (e.g., soil hydrology) or atmospheric (e.g., radiation) models.

The coupled land-atmosphere model has interannual variability in, among other things, temperature and precipitation, which results in large interannual variability in photosynthesis and respiration. In future work, when the terrestrial CO_2 fluxes are used to simulate atmospheric CO_2, this interannual variability could result in significant variability in atmospheric CO_2. Such variability may be a major

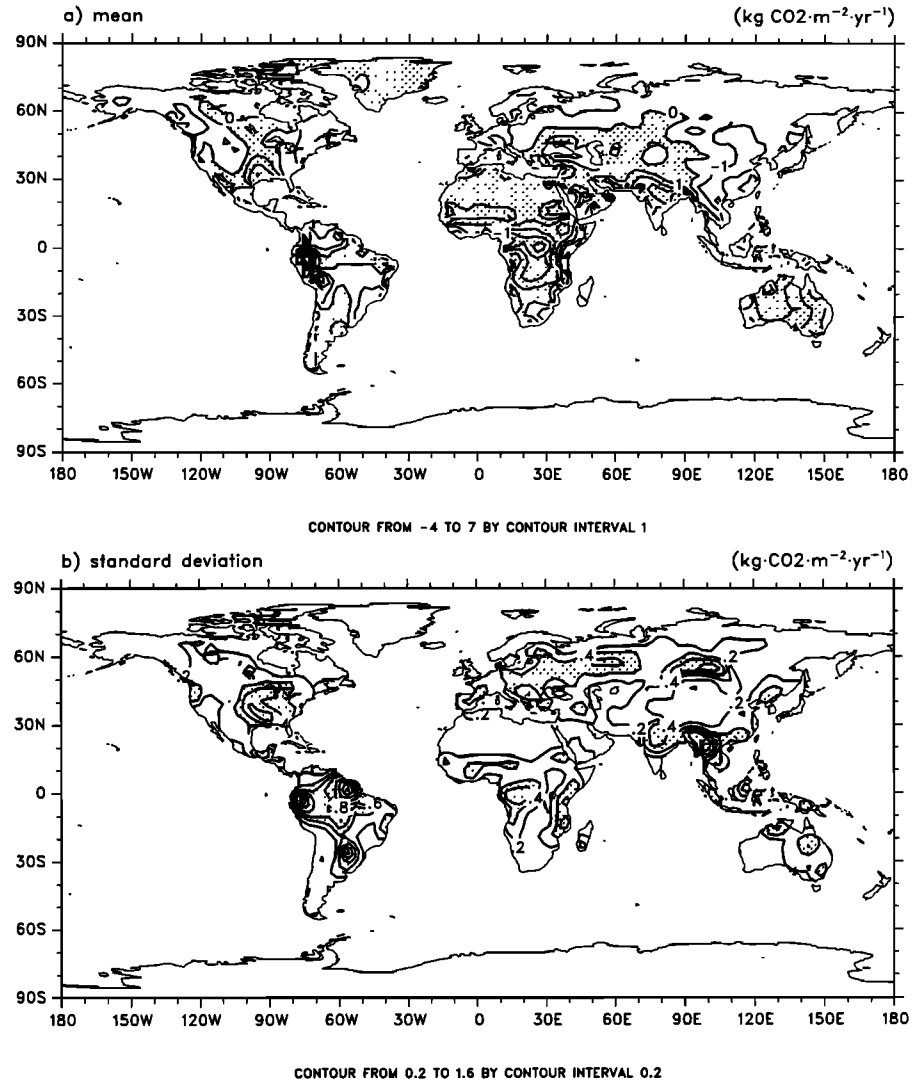

Figure 10. Annual net CO_2 flux (microbial respiration plus plant respiration minus photosynthesis). (a) Five-year mean. Stippling shows areas with a positive flux (i.e., source to atmosphere). (b) Standard deviation. Stippling shows areas >0.4 kg m^{-2} yr^{-1}.

factor in accounting for the "missing" CO_2 sink [*Dai and Fung*, 1993]. This would be in contrast to other analyses in which surface fluxes do not vary from year to year [e.g., *Fung et al.*, 1987].

The model in this study is quite different from other globally implemented models of terrestrial carbon fluxes. These models have a monthly timescale and calculate carbon fluxes from simple relationships with environmental factors, for example, the normalized difference vegetation index and temperature [*Fung et al.*, 1987]; actual evapotranspiration and temperature [*Box*, 1988]; or mean annual air temperature and annual precipitation, with some assumptions about seasonality [*Esser*, 1987; *Friedlingstein et al.*, 1992]. Two recent models have moved beyond these simple approaches to add more physiological and microbial detail to the NPP and soil carbon calculations while maintaining a monthly timescale (Terrestrial Ecosystem Model (TEM) [*Raich et al.*, 1991; *McGuire et al.*, 1992; *Melillo et al.*, 1993] and the Carnegie-Ames-Stanford approach (CASA) biosphere model [*Potter et al.*, 1993]).

Because of the long time step of these models, they are usually run to obtain equilibrium carbon fluxes and pools. In contrast, the model in this study uses prescribed carbon pools (leaf area (L), nonwoody plant biomass (p), soil carbon (a_3)). Moreover, the derivation of the parameters p and a_3 incorporate time-invariant nitrogen and litter quality effects on NPP and microbial respiration, respectively. Hence the applicability of the model is limited to periods in which the carbon and nitrogen pools do vary greatly from year to year. The development of a fully interactive climate systems model requires the addition of long-term changes in carbon and nitrogen pools, vegetation structure, and vegetation composition. Over paleoclimatic timescales these can be added through some type of asynchronous coupling with a potential vegetation model. Over shorter timescales (e.g., 100 years), the ecosystem

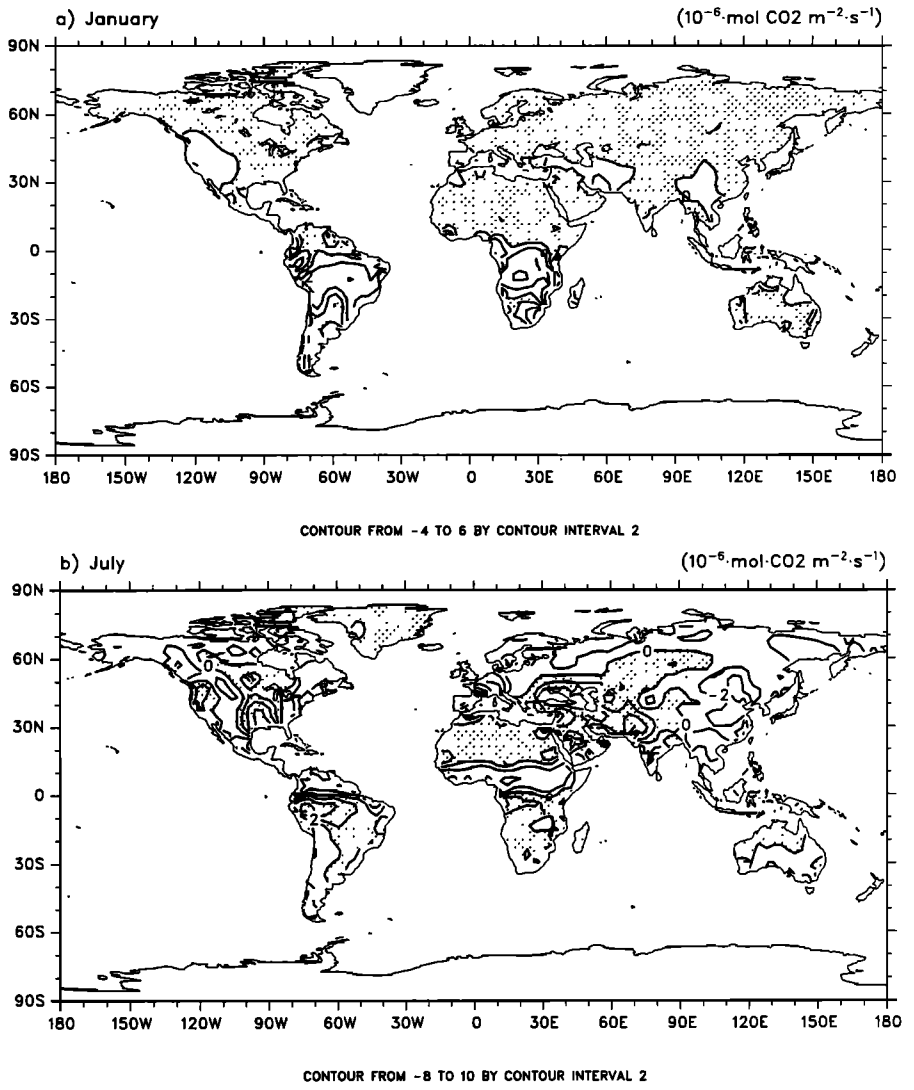

Figure 11. (a) January and (b) July net CO_2 flux (microbial respiration plus plant respiration minus photosynthesis). Stippling shows areas with a positive flux (i.e., source to atmosphere).

dynamics must be consistent with the short-term carbon fluxes.

Despite some of the deficiencies in the current approach, it is seen as a promising means to include biogeochemical fluxes in a climate system model for two reasons. First, it alleviates important discrepancies between the biogeochemical models (monthly time step, simple canopy physiology) and the land surface models (<30 min time step, detailed canopy physiology) typically used in GCMs [*Bonan*, 1993c]. This explicit linking of land-atmosphere energy, water, and CO_2 exchange into a common model has important implications. For example, hydrologists have begun to develop subgrid parameterizations for use with land surface models. Similar subgrid parameterizations are needed for CO_2 exchange, but they must be developed in a manner consistent with the hydrology. Second, the model resolves the diurnal range of CO_2 exchange, which can be large (15–45 μmol CO_2 m^{-2} s^{-1}). In future work, when the terrestrial CO_2 fluxes are used to simulate atmospheric CO_2, this may result in large diurnal variation of CO_2 in the boundary layer, which will feed back to affect photosynthesis and stomatal resistance.

Acknowledgment. The National Center for Atmospheric Research is sponsored by the National Science Foundation.

References

Bonan, G. B., Atmosphere-biosphere exchange of carbon dioxide in boreal forests, *J. Geophys. Res.*, *96*, 7301–7312, 1991.

Bonan, G. B., Physiological controls of the carbon balance of boreal forest ecosystems, *Can. J. For. Res.*, *23*, 1453–1471, 1993a.

Bonan, G. B., Physiological derivation of the observed relationship between net primary production and mean annual air temperature, *Tellus*, *Ser. B*, *45*, 397–408, 1993b.

Bonan, G. B., Do biophysics and physiology matter in ecosystem models?, *Clim. Change*, *24*, 281–285, 1993c.

Bonan, G. B., Comparison of two land surface process models using prescribed forcings, *J. Geophys. Res.*, *99*, 25,803–25,818, 1994.

Box, E. O., Estimating the seasonal carbon source-sink geography of a natural, steady-state terrestrial biosphere, *J. Appl. Meteorol.*, *27*, 1109–1124, 1988.

Bryson, R. A., and F. K. Hare, *World Survey of Climatology*, vol. 11, *Climates of North America*, Elsevier, New York, 1974.

Bunnell, F. L., D. E. N. Tait, P. W. Flanagan, and K. Van Cleve, Microbial respiration and substrate weight loss, I, A general model of the influences of abiotic variables, *Soil Biol. Biochem.*, *9*, 33–40, 1977.

Clapp, R. B., and G. M. Hornberger, Empirical equations for some soil hydraulic properties, *Water Resour. Res.*, *14*, 601–604, 1978.

Collatz, G. J., J. T. Ball, C. Grivet, and J. A. Berry, Physiological and environmental regulation of stomatal conductance, photosynthesis, and transpiration: A model that includes a laminar boundary layer, *Agric. For. Meteorol.*, *54*, 107–136, 1991.

Dai, A., and I. Y. Fung, Can climate variability contribute to the "missing" CO_2 sink?, *Global Biogeochem. Cycles*, *7*, 599–609, 1993.

Dickinson, R. E., A. Henderson-Sellers, and P. J. Kennedy, Biosphere-atmosphere transfer scheme (BATS) version 1e as coupled to the NCAR Community Climate Model, *Tech. Note NCAR/TN-387 + STR*, Natl. Center for Atmos. Res., Boulder, Colo., 1993.

Dorman, J. L., and P. J. Sellers, A global climatology of albedo, roughness length, and stomatal resistance for atmospheric general circulation models as represented by the simple biosphere model (SiB), *J. Appl. Meteorol.*, *28*, 833–855, 1989.

Ducoudré, N. I., K. Laval, and A. Perrier, SECHIBA, a new set of parameterizations of the hydrologic exchanges at the land-atmosphere interface within the LMD atmospheric general circulation model, *J. Clim.*, *6*, 248–273, 1993.

Esser, G., Sensitivity of global carbon pools and fluxes to human and potential climatic impacts, *Tellus, Ser. B*, *39*, 245–260, 1987.

Farquhar, G. D., and S. von Caemmerer, Modeling of photosynthetic response to environmental conditions, in *Encyclopedia of Plant Physiology*, vol. 12B, *Physiological Plant Ecology, II, Water Relations and Carbon Assimilation*, edited by O. L. Lange, P. S. Nobel, C. B. Osmond, and H. Ziegler, pp. 549–587, Springer-Verlag, New York, 1982.

Farquhar, G. D., S. von Caemmerer, and J. A. Berry, A biochemical model of photosynthetic CO_2 assimilation in leaves of C_3 species, *Planta*, *149*, 78–90, 1980.

Foley, J. A., Net primary productivity in the terrestrial biosphere: The application of a global model, *J. Geophys. Res.*, *99*, 20,773–20,783, 1994.

Friedlingstein, P., C. Delire, J. F. Müller, and J. C. Gérad, The climate induced variation of the continental biosphere: A model simulation of the last glacial maximum, *Geophys. Res. Lett.*, *19*, 897–900, 1992.

Fung, I. Y., C. J. Tucker, and K. C. Prentice, Application of advanced very high resolution radiometer vegetation index to study atmosphere-biosphere exchange of CO_2, *J. Geophys. Res.*, *92*, 2999–3015, 1987.

Hack, J. J., B. A. Boville, B. P. Briegleb, J. T. Kiehl, P. J. Rasch, and D. L. Williamson, Description of the NCAR Community Climate Model (CCM2), *Tech. Note NCAR/TN-382 + STR*, Natl. Center for Atmos. Res., Boulder, Colo., 1993.

Hack, J. J., B. A. Boville, J. T. Kiehl, P. J. Rasch, and D. L. Williamson, Climate statistics from the NCAR Community Climate Model (CCM2), *J. Geophys. Res.*, *99*, 20,785–20,813, 1994.

Jones, H. G., *Plants and Microclimate: A Quantitative Approach to Environmental Plant Physiology*, 2nd ed., Cambridge University Press, New York, 1992.

Kiehl, J. T., Sensitivity of a GCM climate simulation to differences in continental versus maritime cloud drop size, *J. Geophys. Res.*, *99*, 23,107–23,115, 1994.

Kiehl, J. T., J. J. Hack, and B. P. Briegleb, The simulated Earth radiation budget of the NCAR CCM2 and comparisons with the Earth Radiation Budget Experiment (ERBE), *J. Geophys. Res.*, *99*, 20,815–20,827, 1994.

Landsberg, J. J., *Physiological Ecology of Forest Production*, Academic, San Diego, Calif., 1986.

Legates, D. R., and C. J. Willmott, Mean seasonal and spatial variability in global surface air temperature, *Theor. Appl. Climatol.*, *41*, 11–21, 1990a.

Legates, D. R., and C. J. Willmott, Mean seasonal and spatial variability in gauge-corrected, global precipitation, *Int. J. Climatol.*, *10*, 111–127, 1990b.

Lieth, H., Modeling the primary productivity of the world, in *Primary Productivity of the Biosphere*, edited by H. Lieth and R. H. Whittaker, pp. 237–263, Springer-Verlag, New York, 1975.

Lydolph, P. E., *World Survey of Climatology*, vol. 7, *Climates of the Soviet Union*, Elsevier, New York, 1977.

McGuire, A. D., J. M. Melillo, L. A. Joyce, D. W. Kicklighter, A. L. Grace, B. Moore III, and C. J. Vorosmarty, Interactions between carbon and nitrogen dynamics in estimating net primary productivity for potential vegetation in North America, *Global Biogeochem. Cycles*, *6*, 101–124, 1992.

Melillo, J. M., A. D. McGuire, D. W. Kicklighter, B. Moore III, C. J. Vorosmarty, and A. L. Schloss, Global climate change and terrestrial net primary production, *Nature*, *363*, 234–240, 1993.

Monteith, J. L., and M. H. Unsworth, *Principles of Environmental Physics*, 2nd ed., Edward Arnold, London, 1990.

Olson, J. S., J. A. Watts, and L. J. Allison, Carbon in live vegetation of major world ecosystems, *Rep. ORNL-5862*, Oak Ridge Natl. Lab., Oak Ridge, Tenn., 1983.

Pitman, A. J., Z.-L. Yang, J. G. Cogley, and A. Henderson-Sellers, Description of bare essentials of surface transfer for the Bureau of Meteorology Research Centre AGCM, *Res. Rep. 32*, Bur. of Meteorol. Res. Cent., Melbourne, Victoria, Australia, 1991.

Potter, C. S., J. T. Randerson, C. B. Field, P. A. Matson, P. M. Vitousek, H. A. Mooney, and S. A. Klooster, Terrestrial ecosystem production: A process model based on global satellite and surface data, *Global Biogeochem. Cycles*, *7*, 811–841, 1993.

Raich, J. W., and W. H. Schlesinger, The global carbon dioxide flux in soil respiration and its relationship to vegetation and climate, *Tellus, Ser. B*, *44*, 81–99, 1992.

Raich, J. W., E. B. Rastetter, J. M. Melillo, D. W. Kicklighter, P. A. Steudler, B. J. Peterson, A. L. Grace, B. Moore III, and C. J. Vörösmarty, Potential net primary productivity in South America: Application of a global model, *Ecol. Appl.*, *1*, 399–429, 1991.

Running, S. W., and J. C. Coughlan, A general model of forest ecosystem processes for regional applications, I, Hydrologic balance, canopy gas exchange and primary production processes, *Ecol. Modell.*, *42*, 125–154, 1988.

Running, S. W., and R. R. Nemani, Relating seasonal patterns of the AVHRR vegetation index to simulated photosynthesis and transpiration of forests in different climates, *Remote Sens. Environ.*, *24*, 347–367, 1988.

Schwerdtfeger, W., *World Survey of Climatology*, vol. 12, *Climates of Central and South America*, Elsevier, New York, 1976.

Sellers, P. J., Y. Mintz, Y. C. Sud, and A. Dalcher, A simple biosphere model (SiB) for use within general circulation models, *J. Atmos. Sci.*, *43*, 505–531, 1986.

Sellers, P. J., J. A. Berry, G. J. Collatz, C. B. Field, and F. G. Hall, Canopy reflectance, photosynthesis, and transpiration, III, A reanalysis using improved leaf models and a new canopy integration scheme, *Remote Sens. Environ.*, *42*, 187–216, 1992.

Verseghy, D. L., CLASS—A Canadian land surface scheme for GCMs, I, Soil model, *Int. J. Climatol.*, *11*, 111–133, 1991.

Verseghy, D. L., N. A. McFarlane, and M. Lazare, CLASS—A Canadian land surface scheme for GCMs, II, Vegetation model and coupled runs, *Int. J. Climatol.*, *13*, 347–370, 1993.

Woodward, F. I., and T. M. Smith, Global photosynthesis and stomatal conductance: Modelling the controls by soil and climate, in *Ecophysiology of Photosynthesis*, edited by E. D. Schulze and M. M. Caldwell, in press, Springer-Verlag, New York, 1994.

Xue, Y., P. J. Sellers, J. L. Kinter, and J. Shukla, A simplified biosphere model for global climate studies, *J. Clim.*, *4*, 345–364, 1991.

G. B. Bonan, National Center for Atmospheric Research, P.O. Box 3000, Boulder, CO 80307-3000.

(Received August 3, 1994; revised October 6, 1994; accepted October 27, 1994.)